Spall size estimation in bearing races based on vibration analysis

G. Kogan[1], E. Madar[2], R. Klein[3] and J. Bortman[4]

[1,2,4]*Pearlstone Center for Aeronautical Engineering Studies and Laboratory for Mechanical Health Monitoring, Department of Mechanical Engineering, Ben-Gurion University of the Negev, P.O. Box 653, Beer Sheva 8410501, Israel*

genak@bgu.ac.il
eyalmad@post.bgu.ac.il
jacbort@bgu.ac.il

[3]*R.K. Diagnostics, P.O. Box 101, Gilon, D.N. Misgav 20103, Israel*

renata.klein@rkdiagnostics.co.il

ABSTRACT

Rolling element bearings are essential components of rotating machinery. Therefore, preventing bearing failure is a subject of great interest. Effective failure prevention requires maintenance decisions that are based on both detection of bearing faults and estimation of the fault severity. Since spalling of raceways is a common bearing failure mechanism, the objective of this study is to estimate the spall width by using vibration analysis.
The ball-spall interaction of faults in both the inner and outer races was studied using a dynamic model of bearings. A new algorithm for determination of the spall width is proposed based on physical insights from the dynamic model. Experimental results are used to validate this algorithm in the case of faults in the outer race.

1. INTRODUCTION

This study continues former research (Mendelovich, Sanders, Kogan, Battat, Klein, Bortman, 2014) that aimed to find indications in the vibration signature of the size of a fault. The ability to assess the bearing condition and to estimate its remaining useful life (RUL) is a key factor for machinery prognostics.

Estimating the bearing RUL requires assessment of the defect severity, i.e. defect size. The manifestation in the vibration signal of a defect located on the inner or the outer ring differs and therefore need to be addressed separately.

Our study focuses on estimating the width of a spall-like fault which is located on one of the raceways in a radially-loaded ball bearing. It is assumed that there is a single fault and that only the inner race is rotating.

A 3D dynamic model (Kogan, Klein, Kushnirsky and Bortman, 2015) is used to simulate faults in the inner and outer rings and to study the effects of fault size and location on the vibration signatures. The simulation results support the development of the proposed algorithm for estimation of the spall size in the outer ring as well as in the inner ring.

The proposed algorithm is validated in tests: bearings are seeded with spall-like faults (Figure 1) with widths between 0.8 mm and 2.5 mm. The fault in the races of the bearing are produced by electro discharge machining, which simulates realistic faults that can often be found in damaged bearings (Mendelovich et al. 2014).

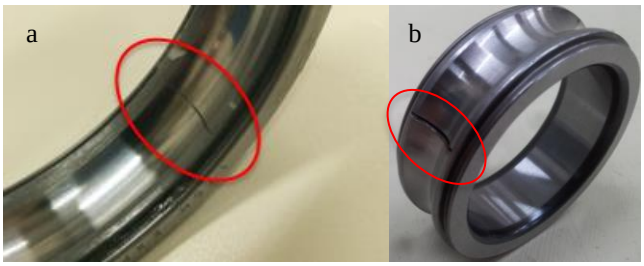

Figure 1. Spall-like fault location in the races: (a) outer (Mendelovich et al. 2014); (b) inner race

2. METHODOLOGY

The investigated method considers the ball-spall interaction. During this interaction, two events occur (Epps, 1991). The first event is the ball entering the spall and the second event is the ball exiting the spall. The system response to these two events depends on the ring that the spall is located in and the distance between them can serve as a good indication for the spall size.

A 3D dynamic ball bearing model is developed (Kogan et al. 2013) to study the effect of faults on the bearing dynamic behavior. For the current study, the contact law of the model

was modified. Based on Gilardi and Sharf (2002), a different stiffness was set for a continuous contact and a contact of colliding bodies.

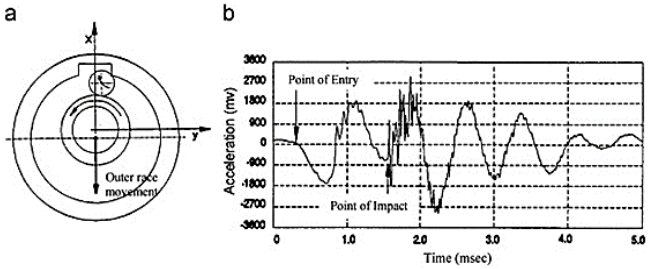

Figure 2. (a) Direction of first movement for the entry motion; (b) a typical acceleration signal measured during the ball-spall interaction (Epps, 1991).

The dynamic model produced an acceleration signal of the outer race for a specific bearing (see Appendix).

2.1. Spall in the outer race

Figure 3 shows a typical acceleration signal (blue) during the ball-spall interaction. The black mark corresponds to the contact of the ball with the entrance edge and the red corresponds to the interaction of the ball with the exit edge.

The first event is the system response to a step function that takes place at the ball entrance into the spall (Figure 3). The second event is the system response to an impulse that takes place at the ball exit from the spall (Figure 3). The simulation shows that the interaction between the ball and the exit edge is not continuous. Before the ball exits the spall, it hits the exit edge several times (the red line in Figure 3) until the ball exists the spall after the last impulse. This phenomenon was reported by Singh, Köpke, Howard, and Petersen (2014), using a detailed finite element analysis for cylindrical rolling elements.

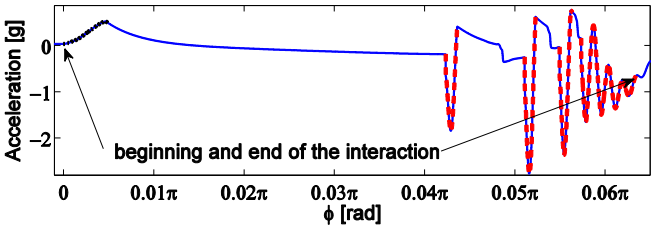

Figure 3. The simulated acceleration of the outer race. Spall in the outer race: blue solid– simulated signal; black doted – ball-entrance edge contact; red – ball-exit edge contact

2.2. Spall in the inner race

Figure 4 and Figure 5 display the simulation results for a case of a bearing with spall located in the inner race. The intensity of the acceleration is higher when the fault approaches the center of the loading zone (Figure 4). Outside the loading zone, the interaction intensity depends on the bearing geometry and the rotation speed. In the considered case, the interaction do not occur outside the loading zone. As a result, each cycle contains only one or two ball-spall interactions.

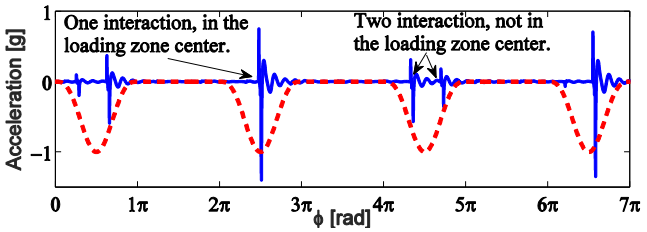

Figure 4. The simulated acceleration of the outer race. Spall in the inner race: blue solid– simulated signal; red dashed– load distribution according to McFadden and Smith, (1984)

Figure 5 shows a typical acceleration signal (blue) during the ball-spall interaction. The black mark corresponds to the contact of the ball with the entrance edge and the red corresponds to the interaction of the ball with the exit edge.

During the interaction the ball rolls around the spall entrance edge and disconnects from the races. As a result, the acceleration signal at the entrance of the ball into the spall is a typical response to a step function.

After the ball disconnection from the entrance edge, the outer race acceleration starts to decay. The gravitation and centrifugal forces might cause the ball to drop back to the outer race and strike several times. The number of strikes depends on the spall width, bearing geometry and the operating conditions.

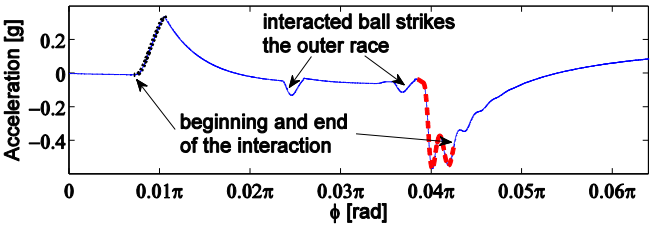

Figure 5. The simulated acceleration of the outer race. Spall in the inner race: blue solid– simulated signal; black doted– ball-entrance edge contact; red dashed– ball-exit edge contact

The exit event in cases of spall located in the inner and outer races differ. In case that the spall is located in the inner ring, the response of the system to the ball exit behaves as a typical response to a step function (Figure 5). Furthermore, in this case the interaction between the ball and the spall exit edge can be considered to be continuous.

In both cases of spalls in the inner and outer race, during the spall-rolling element interaction, two events occur one at the entrance and the second at the exit. In both cases a step response occurs at the entrance of the rolling element into the spall. While the rotating element exits the spall the two cases differ: When the spall is located in the outer race first an impulse response occurs and then the rolling element rattles.

When the spall is in the inner race the exit behaves like a step response.

3. PROPOSED ALGORITHM

The proposed algorithm for estimation of the fault width is based on the measured acceleration signal. It is designed to estimate the width of spall-like faults that are located in the ball path.

The algorithms for spall in the outer and inner races are based on physical understanding of simulations produced with the dynamic model. Additionally, the algorithm works in full autonomy using only parameters based on the bearing geometry and operating conditions of the system. In a preliminary stage the valid and relevant ball-spall interactions are selected. Afterwards, the measured signal is filtered by two filters, one filter to locate the ball entrance into the spall and the other to locate the ball exit from the spall. Then, the algorithm measure the time between the two phenomena. The last phase of the algorithm is to calculate the spall size using the relationship between the measured time and the spall size. The discussed algorithms are shown in Figure 6.

For a spall located on the outer race, a band-passed signal is used to locate the step response that indicates the entrance of the ball into the spall, and a high-passed signal is used to locate the exit of the ball from the spall (Figure 6a). For a spall located on the inner race, two band-passed signals are used to locate the step responses that indicates the entrance of the ball into the spall and the exit of the ball from the spall (Figure 6b). The choice of the band-pass filter cut-off frequencies is based on an approximation of the beginning of the step response to a shifted sine function (Figure 7). The choice of the high-pass filter is based on the estimate of the impact duration. The algorithm is sensitive to the sampling rate and signal-to-noise ratio. A reduction in these parameters affects the estimation reliability.

A typical acceleration signal produced by the dynamic model (Figure 8) illustrates the influence of the limited sampling rate and bandwidth. It shows that the high-frequency content of the acceleration signal during the interaction of the ball with the exit edge is partially masked in the down-sampled signal.

Consequently, the exit of the ball from the spall, which is indicated by the last impulse, is sometimes indistinguishable in the measured acceleration signal. To locate the last impulse, the high-pass filter should be defined to pass frequencies that are significantly higher than the frequencies that are within the range of the band-pass filter.

During each ball-spall interaction, the entrance of the ball is located based on the first local maximum in the band-passed signal (black line in Figure 9) and the exit of the ball is located based on the decay of the last impulse response in the high-passed signal (red line in Figure 9). In each specific interaction, the exit location is approximated by the position of the last instantaneous value that reaches 80% of the maximum absolute amplitude in the acceleration signal.

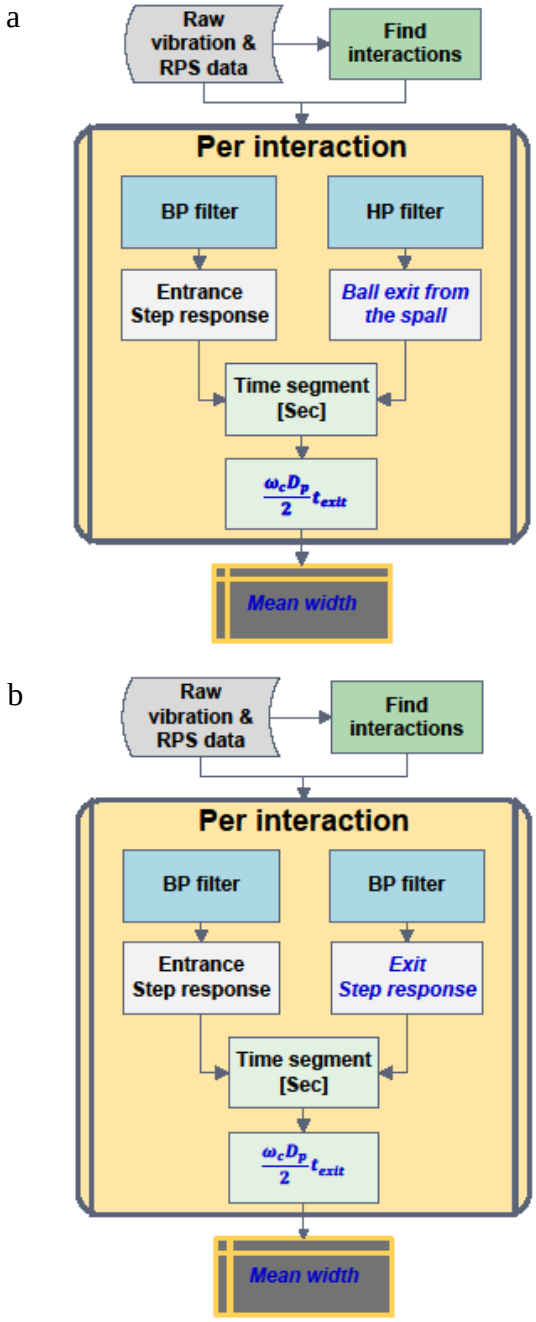

Figure 6. Flow-chart of the algorithms for estimation of the spall size. a: Algorithm to estimate of the spall size in the outer race. b: Algorithm to estimate the spall size in the inner race.

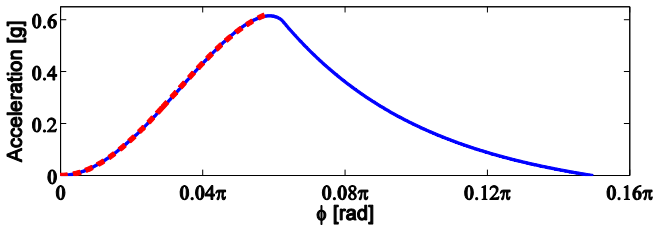

Figure 7. Correlation of the band-pass cut off frequency: blue solid: estimated step response. Red dashed: correlated sine function.

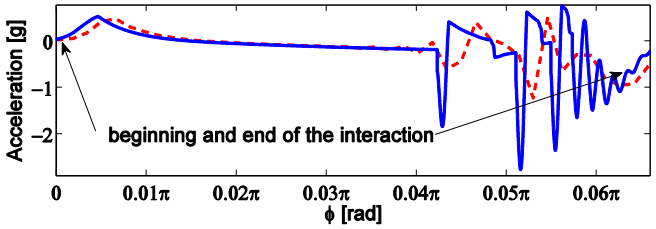

Figure 8. The influence of the sampling rate on a simulated acceleration signal produced during a typical ball-spall interaction: blue solid: original signal; Red dashed: down-sampled signal

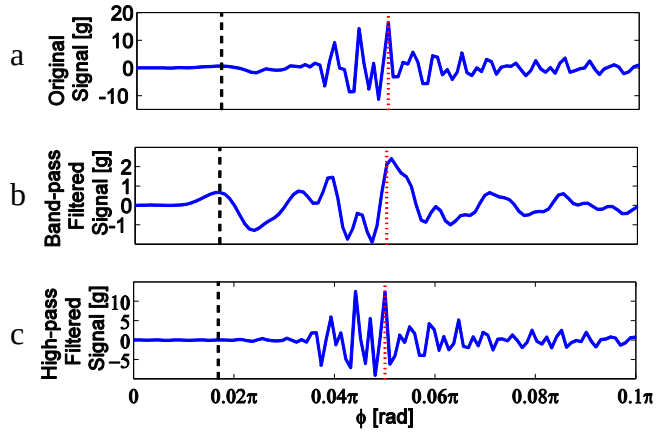

Figure 9. Estimated entrance (black line dashed) and exit (red line dotted) on a measured acceleration signal: (a) original signal; (b) band-passed signal; and (c) high-passed signal

For a spall in one of the races, the distance between the step response and the decay of the rolling element rattling in each ball-spall interaction can be used to estimate the spall width based on the relationship given in (Sawalhi & Randall, 2011):

$$l = \frac{\pi\phi(D_{\mathrm{p}}^2 - d^2)}{2D_{\mathrm{p}}} \quad \ldots\ldots\ldots\ldots\ldots\ldots\ldots (1)$$

where l is the width of the spall, ϕ is the shaft cycle between the step response and the impulse response, D_{p} is the bearing pitch diameter and d is the ball diameter. The proposed algorithm was developed for a radially-loaded ball bearing and might be extended for other cases, such as cylindrical rolling elements Singh et al. (2014). It is assumed that there is one groove-shaped fault located on the ball path in one of the races. The performance of the algorithm might depend on the signal bandwidth, the load, the fault location and shape and the signal-to-noise ratio. It is obvious that the algorithm should be used to estimate the width of the fault upper-bounded by the ball angular distance and lower-bounded by the capability to distinguish between the entrance and the exit of the ball in the signal.

4. TEST

4.1. Test set-up

The experimental system includes two subsystems: a generic test-rig (Figure 10) and a measurement unit. The generic test-rig includes an AC motor and one shaft with two flywheels, mounted on two bearings.

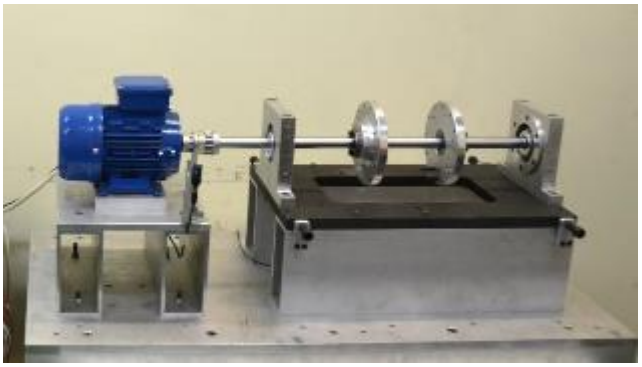

Figure 10. The test-rig

The measurement unit includes a data acquisition system that is connected to an optic sensor and an accelerometer. The optic sensor measures the rotating speed of the shaft and the accelerometer, which is placed on the tested bearing housing (the right bearing housing in Figure 10), measures the vibration signal in the vertical direction. The shaft speed was measured using a Keyence optic sensor and the vibrations were measured using an Endevco 2250A-10 accelerometer. The data was acquired during 60 s, with a sample rate of 25 $\left[\frac{Ksample}{sec}\right]$.

Two bearings were used during each test. The monitored bearing (SKF 6208 ETN9) was installed so that the fault was placed in the center of the loading zone. The fault generation process is described in detail in Mendelovich et al. (2014). 15 different bearings were monitored: one healthy and 14 with different fault sizes in the outer race.

4.2. Results of the proposed algorithm

The implementation of the algorithm on the measured acceleration signal estimated the fault width with relatively

small errors (Figure 11). However, the estimation of the small faults (with widths of 0.78 mm) had large errors.

An analysis of the simulation results provided a possible explanation. Figure 12 shows that in the case of small spalls, the limited frequency range and sampling rate 'filter out' all of the impacts from the measured acceleration signal. Therefore, all of the algorithms based on the identification of the entrance and exit of the ball in and out of the fault area will probably present the same limitation.

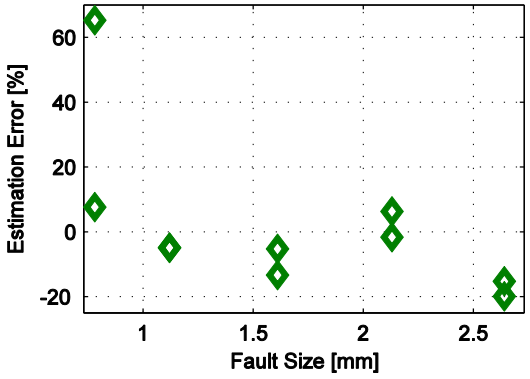

Figure 11. Relative error of the algorithm estimated width versus the optical measurements of the fault width as a function of the fault width.

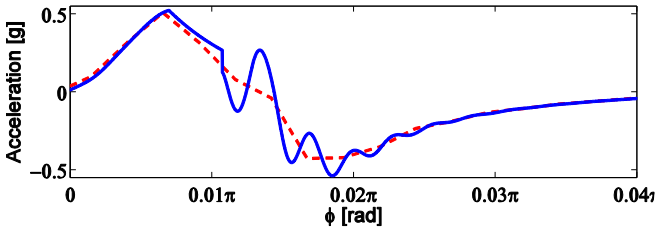

Figure 12. The influence of the sampling rate on a simulated acceleration signal during the interaction of the ball with a 0.6 mm-width spall: blue solid – original acceleration signal; red dashed– down-sampled signal

5. SUMMARY

Effective failure prevention requires maintenance decisions that are based on both a diagnosis of bearing faults and an estimation of the severity of the fault.

Faults of different sizes both in the outer and inner race were simulated using a well-established dynamic model of a bearing. Based on the insights obtained from the simulations, a new algorithm for fault width estimation was developed. The algorithm was demonstrated for bearing tests with faults in the outer race.

The dynamic model explains the lower-bound of the size of a detectable fault considering the influence of the signal bandwidth.

A set of seeded fault tests (fault widths from 0.8 mm to 2.5 mm) was carried out in order to validate the proposed algorithm. For faults wider than 0.8 mm, the algorithm shows satisfactory results, with errors below 20%.

A future study will validate the algorithm for faults in the inner race and will investigate the sensitivity of the algorithm to additional parameters, such as signal-to-noise ratio, fault location and shape, bandwidth, load and bearing type.

Acknowledgements

The authors gratefully acknowledge the invaluable support of Tal Yehoshua. They would also like to thank the Pearlstone Foundation.

REFERENCES

Epps, I. (1991). An investigation into vibrations excited by discrete faults in rolling element bearings (Unpublished doctoral dissertation). University of Canterbury. Mechanical Engineering.

Gilardi, G., & Sharf, I. (2002). Literature survey of contact dynamics modelling. Mechanism and machine theory, 37(10), 1213–1239.

Kogan, G., Klein, R., Kushnirsky, A., & Bortman, J. (2015). Toward a 3d dynamic model of a faulty duplex ball bearing. Mechanical Systems and Signal Processing, 54, 243–258.

McFadden, P., & Smith, J. (1984). Model for the vibration produced by a single point defect in a rolling element bearing. Journal of sound and vibration, 96(1), 69–82.

Mendelovich, M., Sanders, Y., Kogan, G., Battat, M., Klein, R., & Bortman, J. (2014). Characterization of fault size in bearings. Annual conference of the Prognostics and Health Management Society, Fort Worth, Texas, September 2014.

Sawalhi, N., & Randall, R. (2011). Vibration response of spalled rolling element bearings: Observations, simulations and signal processing techniques to track the spall size. Mechanical Systems and Signal Processing, 25(3), 846–870.

Singh, S., Köpke, U. G., Howard, C. Q., & Petersen, D. (2014). Analyses of contact forces and vibration response for a defective rolling element bearing using an explicit dynamics finite element model. Journal of Sound and Vibration, 333(21), 5356–5377.

APPENDIX

The simulated case is a bearing with a spall-like fault located in the raceway of one of the races. For the outer race the fault located in the center of the loading zone. The simulation was carried out for a spall width from zero (no spall) to 3 mm with increments of 0.1 mm. The simulation parameters are detailed in Table 1.

Table 1. Model parameters for the simulated cases.

Pitch diameter	$60[\ mm\ ]$
Ball diameter	$12[\ mm\ ]$
Inner raceway normalized curvature	0.52
Outer raceway normalized curvature	0.53
Contact stiffness exponent	1.5
Friction coefficient	0.16
Clearance diameter	$1.5\ \cdot\ 10-2\ [\ mm\ ]$
Number of balls	9
Modulus of elasticity for balls and rings	$208[\ Gpa\ ]$
Ball mass	$6.5[\ gr\ ]$
Mass attached to the inner ring	$14.37[\ kg\ ]$
Mass attached to the outer ring	$9.5[\ kg\ ]$
Outer ring-world radial spring	$106\ [\ N/m\ ]$
Outer ring-world radial damper	$105\ [\ N\cdot s/m\ ]$
Radial gravity	$9.81[\ m/s2\ ]$
Inner ring rotation speed	$20[\ rps\ ]$
Time step	$2.5\ \cdot\ 10^{-7}\ [s]$
Ball-inner ring contact-stiffness	$3.25\ \cdot\ 1010\ [\ n/m1.5\ ]$
Ball-outer ring contact-stiffness	$2.84\ \cdot\ 1010\ [\ n/m1.5\ ]$